CrossMark

ORIGINAL CONTRIBUTION

Preparation of metal ion-mediated Furosemide molecularly imprinted polymer: synthesis, characterization, and drug release studies

Amir Reza Fareghi[1] · Peyman Najafi Moghadam[1] · Jabbar Khalafy[1]

Abstract In the present study, a molecularly imprinted polymer (MIP) was prepared for Furosemide drug as template molecule in H_2O/THF (1:1 v/v) medium using Fe^{3+} as metal ion mediator. Acrylic acid, acrylamide, and N,N'-methylenebis(acrylamide) were used as functional monomer, comonomer, and cross-linking agent, respectively. Different binding and selectivity parameters of the prepared system were studied and compared with the corresponding metal ion-free MIP and non-imprinted polymer (NIP). The presence of the metal ion during pre-assembly step showed a significant influence on the imprinting ability of the resulting polymeric network due to its strong interactions with the template molecule and the functional monomer. Besides, structural, thermal, and morphological characterizations of the prepared system were investigated. In the final step, the in vitro release study of Furosemide from the synthesized polymers was carried out in pH = 7.41 phosphate-buffered saline solution at 37 °C. Results indicated that the Fe^{3+}-mediated MIP (Fe-MIP) has larger drug loading capacity and higher amount of drug release at its equilibrium state. Moreover, according to the drug release profiles, the drug release rate of the Fe-MIP is more controlled than that of the MIP and the NIP, especially at the early stages of release.

Introduction

In recent years, the molecular imprinting technology has attracted much more attention due to its widespread applications. The resulting molecularly imprinted polymer (MIP) as a macromolecular network has specific binding sites to recognize the target molecule named as template [1].

To prepare MIPs, a typical synthesis route is the radical polymerization of functional monomer(s) pre-assembled around the template in the presence of a suitable cross-linker monomer [2]. The cross-linker monomer fixes the pre-assembled monomer(s) in a spatial arrangement and retains the shape of the resulting polymeric network. Then, the template is removed from the MIP structure and results in shape-specific cavities matching the template molecule [3].

To date, many researches have been published developing imprinting protocols in different fields such as chiral separation [4], solid-phase extraction (SPE) [5], chemical catalysis [6], and drug delivery systems [7]. Most of the developed protocols in the molecular imprinting technology are produced in organic solvents [8, 9] due to their lower polarity and hydrogen bonding ability compared to aqueous media. The higher polarity and hydrogen bonding ability of water compete with functional monomer(s) to assemble around the template and reduce the recognition ability of the MIP toward the template molecule [10]. However, due to the undeniable advantages of water as a green, non-toxic, and abundant solvent (which is especially important in the field of drug delivery), researchers are seeking ways to employ water in the preparation of MIPs. By now, a number of successful MIP

✉ Peyman Najafi Moghadam
p_najafi27@yahoo.com

Amir Reza Fareghi
amir_fareghi@yahoo.com

Jabbar Khalafy
jkhalafi@yahoo.com

1 Department of Chemistry, Faculty of Science, Urmia University, Urmia, Iran

preparations in aqueous or water/organic solvent media have been reported [11, 12].

One of the most common solutions to avoid the disturbance caused by water during polymerization is to use metal ions as mediators in the pre-assembly step [13]. In these systems, stronger ionic interactions created between monomer-metal ion and template-metal ion replace the unwanted hydrogen bonding [14].

Furosemide (Fig. 1a), systematically named as 5-(aminosulfonyl)-4-chloro-2-([2-furanylmethyl]amino)benzoic acid, is a highly effective and quick-acting diuretic drug whose action, like all of the examined loop diuretics, is associated with blocking reabsorption of ions in the ascending bend of Henle's loop [15]. This medication is used for the treatment of congestive heart failure [16], chronic renal failure [17], and cirrhosis of the liver [18]. But as a conventional treatment, it is used for the treatment of high blood pressure [19, 20].

Besides serious side effects of Furosemide including electrolyte abnormalities and hearing loss, the most common side effect is sudden decrease in blood pressure [21]. Hence, the controlled usage of this drug is necessary.

The employment of slow release systems is one of the most prevalent ways to control the released amount of drug. There are some researches published about Furosemide slow release [22, 23], but only a few publications are about the employment of molecular imprinting technology [24].

In this study, a Furosemide-imprinted drug delivery system was prepared using acrylic acid (AA) and acrylamide (AAm) as the functional monomer and comonomer, N,N'-methylenebis(acrylamide) (MBAAm) as the cross-linking agent, and Fe^{3+} ions as the mediator in H_2O/tetrahydrofuran (THF) (1:1 v/v) medium. The effect of the mediator on the binding ability and selectivity of the prepared system was investigated and compared with the corresponding Fe^{3+}-free MIP and non-imprinted polymer (NIP) in different parts of the study. Finally, the in vitro release study of Furosemide was carried out from the synthesized carriers. In order to simulate the normal arterial blood pH value and normal body temperature, the release study was performed in pH = 7.41 phosphate-buffered saline (PBS) solution at 37 °C.

Experimental

Materials

AA (≥99% Merck) was distilled under reduced pressure before use, and α,α'-azobis(isobutyronitrile) (AIBN) (≥98% Merck) was recrystallized from hot (50 °C) methanol and kept away from light before use. AAm (≥99% Merck) and MBAAm (≥98% Merck) were used without further purification. Furosemide (FR) (MW = 330.74) (20 mg/2 ml vials, 10,000 ppm solutions in deionized water) (Alborz Darou Pharmaceutical Co., Qazvin, Iran), Midazolam (MD) (MW = 325.77) (5 mg/1 ml vials, 5000 ppm solutions in deionized water) (Tehran Chemie Pharmaceutical Co., Tehran, Iran), and Salbutamol (SL) (MW = 239.31) (0.5 mg/ 1 ml vials, 500 ppm solutions in deionized water) (Exir Pharmaceutical Co., Boroujerd, Iran) were used as received. The chemical structures of the drugs are depicted in Fig. 1. Diluted solutions of the drugs were prepared from the above-mentioned stock solutions. For swelling and in vitro drug release studies, PBS solution (0.01 M, pH = 7.41) was used as the medium.

Apparatus and software

The FT-IR and UV-Vis spectra were recorded by Thermo Nicolet NEXUS 670 FT-IR (Thermo Scientific, USA) and Agilent 8453 Diode Array UV-Vis spectrophotometer (Agilent Technologies, USA), respectively. The cyclic voltammetry (CV) analysis was performed with SAMA 500 Electroanalyzer System (Sama Research Center, Iran). The scanning electron microscopy (SEM) images were obtained from LEO 1430 VP (Leo Electron Microscopy Ltd., UK). The thermogravimetric analysis (TGA) was studied by STA PT1000 TG-DSC (STA Simultaneous Thermal Analysis) STA (TG-DSC/DTA) Thermogravimetric Analyzer (Linseis Thermal Analysis, Germany) at a heating rate of 10 °C/min under N_2 atmosphere. The equilibrium concentration of components in competitive media was estimated using the multivariate curve resolution-least squares (MCR-LS) method which was performed on MATLAB R2015a (8.5).
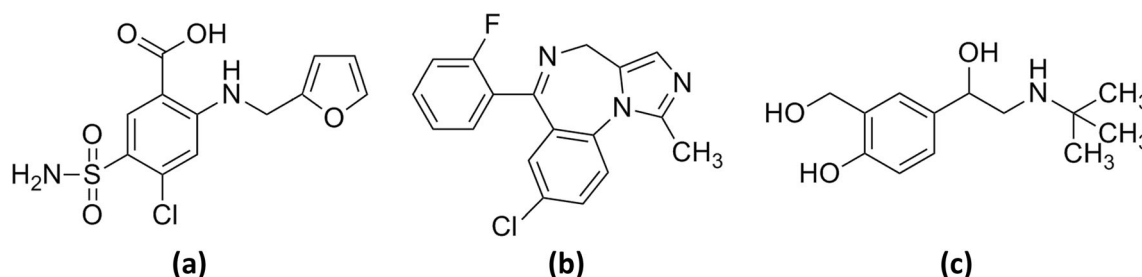

Fig. 1 The chemical structures of **a** Furosemide (FR), **b** Midazolam (MD), and **c** Salbutamol (SL)

Synthesis of the MIPs and NIP

The amounts of chemicals used to synthesize the MIPs and the NIP are according to Table 1. The synthesis route for the preparation of the metal ion-free MIP is as follows: firstly, a solution of 40 mg FR in 10 ml H_2O/THF (1:1 v/v) mixture was prepared in a 25 ml two-necked round-bottom flask. Then, AA was added to the solution and the mixture was stirred for 2 h at room temperature to complete the pre-assembly step. AAm and MBAAm were then added to the pre-assembly solution and the solution was degassed with argon for 20 min to remove the dissolved oxygen followed by adding AIBN to the degassed solution. The polymerization reaction was completed after 8 h at 60 °C under inert atmosphere. The resulting bulk rigid polymer was crushed, ground into fine powder, and washed with distilled water and acetone several times. The template molecule was extracted from the polymer structure using acetone in a Soxhlet extraction system during 24 h. The corresponding NIP was prepared in the absence of the template using the same procedure.

In order to synthesize the Fe^{3+}-mediated MIP (Fe-MIP), a 0.25-M solution of $FeCl_3 \cdot 6H_2O$ in distilled water was prepared first. Then, a total amount of 10 ml H_2O/THF (1:1 v/v) solution containing Fe^{3+}, AA, and FR was prepared by adding 1 ml of the Fe^{3+} solution into 5 ml of THF in a 25-ml two-necked round-bottom flask followed by adding AA. After an hour of stirring, 4 ml of FR solution (40 mg of FR) was added to the mixture. The final solution was let to be stirred for additional 2 h at room temperature to complete the pre-assembly step. Then, the procedure was continued as described for the MIP. The final polymer, after crushing and grinding, was introduced into 100 ml of HCl solution (1 M) and stirred for 48 h at room temperature until complete removal of Fe^{3+} from the polymer structure. The template was then extracted as described above.

Cyclic voltammetry

Cyclic voltammetry analysis was carried out in order to prove whether Fe^{3+} ions bridged between the template (FR) and the functional monomer (AA). For this purpose, three different solutions containing pure Fe^{3+}, Fe^{3+} with AA (Fe-AA), and Fe^{3+}, AA, and FR (FR-Fe-AA) were prepared and analyzed. The latter solution was prepared by adding the drug to the premixed Fe-AA solution to ensure that the ternary complex has been formed. The experimental conditions were as follows: platinum plate electrodes with electrochemically active surface area of 6 and 9 cm^2 were used as working and auxiliary electrodes, respectively, and Ag/AgCl was used as reference electrode. The scanning potential range was set between 200 and 700 mV with the scan rate of 20 mV s^{-1}.

Swelling studies

The swelling behavior of the polymers was studied in pH = 7.41 PBS solution. Briefly, 10 mg of each polymer was weighed precisely and placed into separate pre-weighed wet tea bags. Then, the tea bags were immersed in 200 ml of the buffer solution. At specific time intervals, the tea bags were lifted from the solution and reweighed. The swelling ratios (SRs) were calculated from the equation as follows:

$$SR = \frac{(W_t - W_1 - W_0)}{W_1}$$

where the W_t, W_1, and W_0 represent the total weight of swollen polymer and wet tea bag at the specified time, the weight of dry polymer, and the weight of wet tea bag, respectively.

The equilibrium swelling ratio (ESR), which is attributed to the amount of water absorbed by polymer at equilibrium state, was also calculated by the same equation, except W_{eq} that was placed instead of W_t, referring to the total weight of swollen polymer and wet tea bag at equilibrium state (no changes in weight over time). The ESR values are shown in Table 3.

$$ESR = \frac{(W_{eq} - W_1 - W_0)}{W_1}$$

Equilibrium binding studies

In order to study the equilibrium binding capacity, 10 mg of each polymer was added into 20 ml of FR solutions ranging

Table 1 Composition of the samples

Sample	Template[a] (mg)	AA (mg)	AAm (mg)	MBAAm[b] (mg)	Fe^{3+c} (ml)	AIBN[d] (mg)
Fe-MIP	40.00	34.86	34.39	372.91	1.00	1.59
MIP	40.00	34.86	34.39	372.91	–	1.59
NIP	–	34.86	34.39	372.91	–	1.59

[a] The molar ratio of the template to each of the monomers is 1:4

[b] The molar ratio of the template to MBAAm is 1:20

[c] The molar ratio of Fe^{3+} to AA is approximately 1:2

[d] The amount of AIBN is 2 mol% of AA

from 1 to 80 ppm (3.02 to 241.88 μmol l^{-1}) in 50-ml glass vials. The vials were sealed and slowly shaken overnight at room temperature, and then each solution was filtered and centrifuged for 10 min at 4000 rpm. The supernatants were analyzed by UV-Vis spectrophotometer at 330 nm according to the FR UV-Vis spectrum (Fig. 7a). The binding parameters of the polymers were further processed using the Scatchard equation defined as follows:

$$\frac{Q}{C_s} = \frac{Q_{max} - Q}{K_d}$$

where Q (μmol.g^{-1}) is the equilibrium adsorption capacity (amount of template bound to the sorbent), C_s (μmol l^{-1}) is the equilibrium concentration of template in solution, Q_{max} (μmol g^{-1}) is the maximum binding capacity (maximum number of binding sites), and K_d (μmol l^{-1}) is the dissociation constant. The K_d and Q_{max} can be estimated from the slope and y intercept of the Scatchard plot (Q/C_s versus Q) (Fig. 10). The Q was also calculated from the equation as follows:

$$Q = (C_i - C_s)\left(\frac{V}{m}\right)$$

where C_i (μmol l^{-1}) is the initial concentration of the solution, V (l) is the volume of the solution, and m (g) is the amount of the sorbent. The Scatchard analysis data are shown in Table 3.

Selectivity studies

To study the selectivity of the MIPs and the NIP, MD and SL drugs were selected as competitive molecules. For this purpose, for each of the polymers, two binary mixtures containing FR-MD and FR-SL and a ternary mixture containing FR, MD, and SL were prepared. The concentration of each component was 10 ppm. To carry out the experiment, 10 mg of the polymer was introduced into 20 ml of each solution in 50-ml glass vials. The vials were sealed and slowly shaken for 24 h at room temperature. Then, the solutions were filtered and centrifuged for 10 min at 4000 rpm, and the supernatants were analyzed. The distribution constant (K_D) which reflects the migration and separation capacity of a solute in two phases is defined as follows:

$$K_D = \left(\frac{C_i - C_f}{C_f}\right)\left(\frac{V}{m}\right)$$

K_D (l g^{-1}), C_i, and C_f (μmol l^{-1}) represent the distribution constant, the initial, and equilibrium concentration of each component, respectively. Also, V (l) and m (g) demonstrate the volume of the solution and the amount of the sorbent, respectively. The selectivity coefficient (k) which shows the selectivity of a component toward other component(s) for a specific sorbent was calculated from the following equation:

$$k = \frac{K_{D\ (template)}}{K_{D\ (analogue)}}$$

The relative selectivity coefficient (k') of the template for the Fe-MIP and the MIP against the NIP was further calculated for each of the binary and ternary mixtures using the equation below:

$$k' = \frac{k_{MIP}}{k_{NIP}}$$

The selectivity data are shown in Tables 4, 5, and 6.

Drug loading and in vitro release studies

To carry out the loading process for each of the polymers via soaking procedure, 4 ml of the 10,000 ppm FR solution was introduced into separate falcon conical centrifuge tubes. Then, a precisely weighed amount of each polymer was added into the tubes and the tubes were kept in the dark and agitated slowly for 48 h at room temperature until complete uptake of the drug. The loaded polymer was then collected via centrifugation and washed with distilled water to remove any surface-adhered drug, and then dried at room temperature.

To calculate the loading capacity (LC), the loaded polymer was reweighed after complete drying. Therefore, the net weight of the drug could be determined by weight subtraction of the loaded and unloaded polymer. The loading capacity percentage (LC%) was calculated using the following equation:

$$LC\% = \frac{W}{W'} \times 100$$

where the W is the net weight of the drug and W' is the weight of the dry polymer before loading. The LC% data are shown in Table 7.

In order to determine the imprinting factor (IF) of the two MIPs toward the NIP, the partition coefficient (P) was calculated for each of the polymers from the equation as follows:

$$P = \frac{Q}{C_s}$$

The Q and C_s are defined in the "Equilibrium binding studies" section. The IFs were further determined from the following equation:

$$IF = \frac{P_{MIP}}{P_{NIP}}$$

The P and IF values are also shown in Table 7.

To study the in vitro release process, 20 mg of the loaded polymer was introduced into a dialysis tube and immersed in a

vial containing 50 ml of pH = 7.41 PBS solution placed in a thermostatic bath adjusted at 37 °C without stirring. At specific time intervals, the supernatant was analyzed with UV-Vis spectrophotometer at 330 nm. The release diagram of the drug for each of the polymers was drawn in the form of cumulative drug release percentage as a function of time (Fig. 12).

Results and discussion

Preparation of the MIPs and the NIP

The key step in the preparation of a successful MIP is the formation of an appropriate complex between the template and the functional monomer. In the present paper, Fe^{3+} ions were employed as a mediator to bridge between the template (FR) and the functional monomer (AA) in order to enhance the complex formation. To prove this claim in which the Fe^{3+} ions have successfully played the role of a mediator, cyclic voltammetry analysis was carried out. Since Fe^{3+} ions are electroactive species, the coordination of any ligand and formation of complex causes a negative shift in the reductive peak potential demonstrating higher negative potential to reduce Fe^{3+} ions. The larger negative shift in the reductive peak potential indicates higher stability of the formed complex. Figure 2 shows the cyclic voltammograms of the Fe^{3+}, the Fe-AA, and the FR-Fe-AA solutions, and Table 2 shows the related data. As shown in this figure, the negative shift is observable in the reductive peak potential through the formation of the complex between AA and Fe^{3+} ions ($\Delta E = -41$). A larger negative shift is also found for the FR-Fe-AA complex ($\Delta E = -87$) suggesting a successful and more stable ternary complex formation before polymerization.

To compare the efficiency of the metal ion-mediated complex formation against conventional method which is the hydrogen bond complex formation, the metal ion-free MIP was also prepared. Different parameters such as binding, selectivity, swelling, drug loading, and in vitro release behaviors of
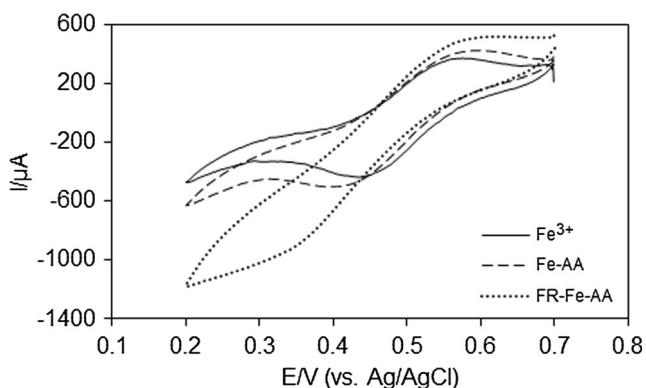

Fig. 2 Cyclic voltammograms of Fe^{3+}, Fe-AA, and FR-Fe-AA

Table 2 Cyclic voltammetry analysis data

Sample	Reductive peak potential (mV)	ΔE^a (mV)
Fe^{3+b}	435	–
Fe-AA[c]	394	−41
FR-Fe-AA[c]	348	−87

[a] $\Delta E = E - E(Fe^{3+})$

[b] 5 mM solution in H_2O/THF (1:1), KCl (0.1 M) as the supporting electrolyte

[c] 5 mM solution of Fe^{3+} in H_2O/THF (1:1) with the same molar ratios as described in Table 1, KCl (0.1 M) as the supporting electrolyte

the prepared Fe-MIP were investigated alongside with the MIP and the corresponding NIP which are further discussed in the following sections.

Structural characterization

Figure 3 shows the FT-IR spectrum of the Fe-MIP. The sharp absorption band at 1657 cm^{-1} is attributed to the amidic carbonyl groups, and the band at 2940 cm^{-1} is related to the C-H bond stretching vibrations. The N-H bond stretching and bending vibrations are also appeared at 3424 and 1527 cm^{-1}, respectively. It is noteworthy to mention that the absorption band of acidic carbonyl groups related to AA is overlapped with the amidic carbonyl groups due to their lower amount present in the polymer structure compared to the amidic carbonyl groups of both MBAAm and AAm. But on the other hand, the broadening of absorption bands in the region between 2700 and 3700 cm^{-1} could be as a result of the –COOH presence in the polymer structure.

To investigate the thermal stability of the prepared system, TGA analysis was carried out. Figure 4 shows the TGA thermogram of the Fe-MIP. As shown in this figure, the prepared polymer is thermally stable up to 300 °C. Above this temperature, two-step degradation is observable. The first degradation step between 300 and 450 °C is attributed to the disjunction of cross-linking and pendant groups which cause the emission of CO, CO_2, and NH_3. The main backbone of the polymer is destructed above 450 °C up to about 700 °C.

In order to study and compare the surface morphology of the prepared polymers, SEM technique was employed. Figure 5 shows the SEM images of the samples. As shown in Fig. 5a, which is related to the Fe-MIP, a rather uniform structure with compact globular particles and almost equal-shaped cavities is observable. This could be as a result of the metal-ion mediation in which the stable complex formation caused isometric cavities after the template removal. Figure 5b shows the SEM image of the MIP. As shown in this figure, the rock-shaped structure with unequal-sized cavities is indicative

Fig. 3 FT-IR spectrum of Fe-MIP
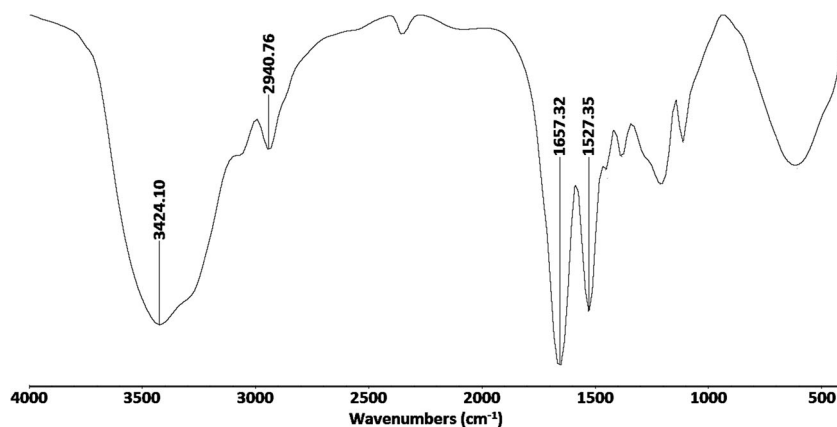
of an inappropriate interaction between FR and AA during pre-assembly step, compared to the Fe-MIP. Also, Fig. 5c shows the SEM image of the NIP. In this figure, a very tough and flat surface is observable. This could be due to the high amount of cross-linker and the absence of the template which caused a rigid structure with tiny cavities.

Besides binding and selectivity, the morphological structures of the polymers affect directly on the swelling behavior and subsequently on the drug loading and releasing. These behaviors are discussed in the following sections.

Swelling studies

Swelling behavior is one of the key parameters in polymeric drug carriers used in the controlled drug delivery. Based on Flory's network theory [25], water absorption and SR in a polymeric network are functions of cross-linker density. In the molecular imprinting technology, since higher amounts of cross-linker is used in order to reach a rigid structure with stable pore shapes, lower SRs in these systems are inevitable. On the other hand, lower SRs reduce the drug loading capacity of polymers due to smaller pore sizes. Therefore,

there should be a balance between the SR and the rigidity for the MIPs used in drug delivery systems. One of the solutions to overcome this issue is to use a comonomer alongside with the main functional monomer. AAm is a very suitable comonomer which is used with AA to improve the swelling behavior [26]. According to Yao et al. [27], copolymerization of AA with AAm in lower molar ratios of AAm to AA enhances the SR in distilled water due to the collaborative effect of $-CONH_2$ and $-COO^-$ groups. By increasing the molar ratio of AAm to AA, the SR decreases because the number of $-COO^-$ groups as ionic and more hydrophilic species reduces in the resulting polymer structure. In saline solutions, higher molar ratios of AAm to AA increase the SR. In these solutions, the cationic counterion (Na^+, K^+, Ca^{2+}, etc.) interacts with the ionized $-COO^-$ groups, reduces the negative charge repulsion, and leads to the lower SRs, the so-called "charge screening effect" phenomenon [28]. In our study, PBS medium as a saline solution with pH = 7.41 was used in order to simulate the normal body pH value. Therefore, to improve the swelling behavior of the prepared polymers, an equal molar ratio of AAm to AA was selected.
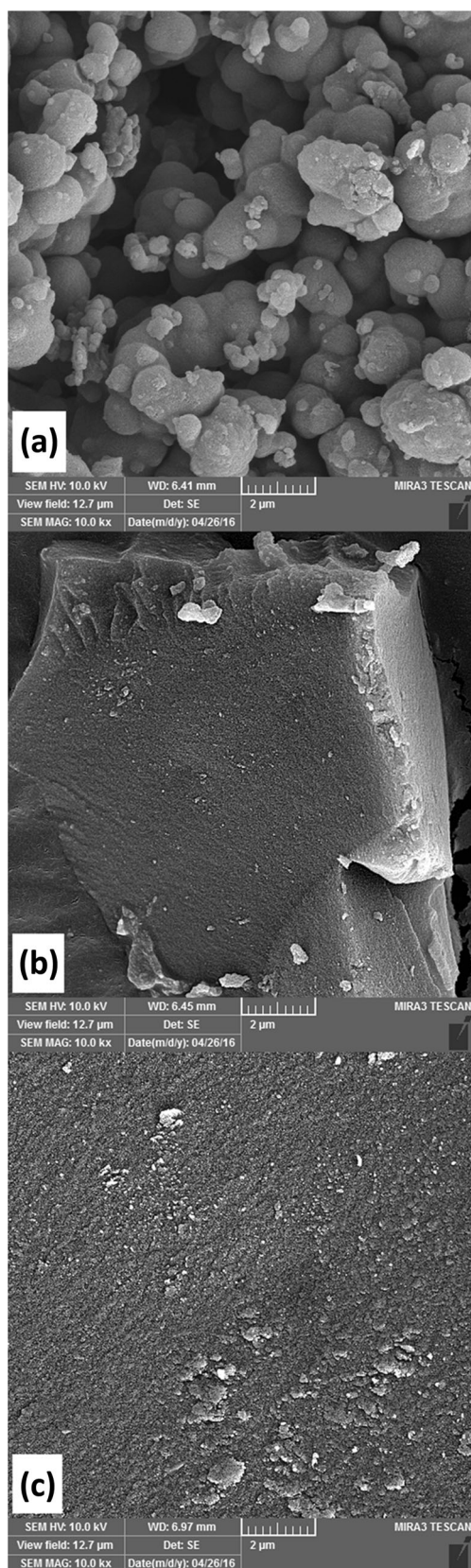
Fig. 4 TGA thermogram of Fe-MIP
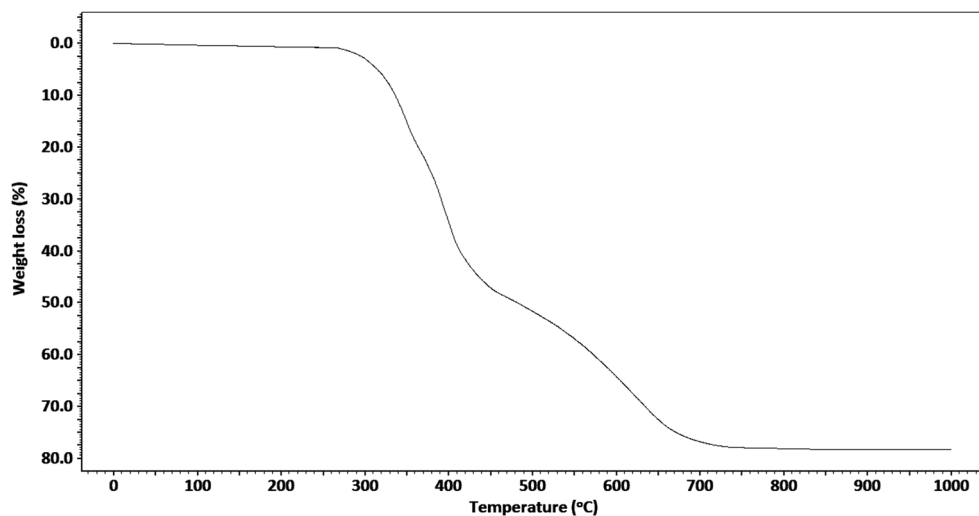
Fig. 5 SEM images of **a** Fe-MIP, **b** MIP, and **c** NIP

Figure 6 shows the swelling diagrams of the polymers during 5 h and 2 days, respectively. As shown in this figure, the water uptake is increased as a function of time for all of the samples, but the NIP reaches to the relatively lower SRs. This can be attributed to the tiny cavities in the NIP structure (Fig. 5c) which leads to absorb less water. The template removal after the MIP preparation leaves larger cavities in the polymer structure; hence, it is expected that MIPs show higher SRs than NIPs. As shown in Fig. 6, both the Fe-MIP and the MIP show higher SRs than the NIP, and the higher SR of the Fe-MIP is attributed to the more regular pore shapes and the presence of Fe^{3+} ions during polymer preparation which leads to remain larger cavities after the template and metal ion removal. The highest SR which is achieved at the equilibrium state ratio (ESR) is calculated for each of the samples, and the related values are shown in Table 3.

Equilibrium binding studies

To determine the equilibrium adsorption capacity (Q) of the samples in solutions with various FR concentrations, firstly, the UV-Vis spectrum of FR (5 ppm solution) was obtained (Fig. 7a). From the UV-Vis spectrum, the corresponding calibration curve was plotted at 330 nm (Fig. 8).
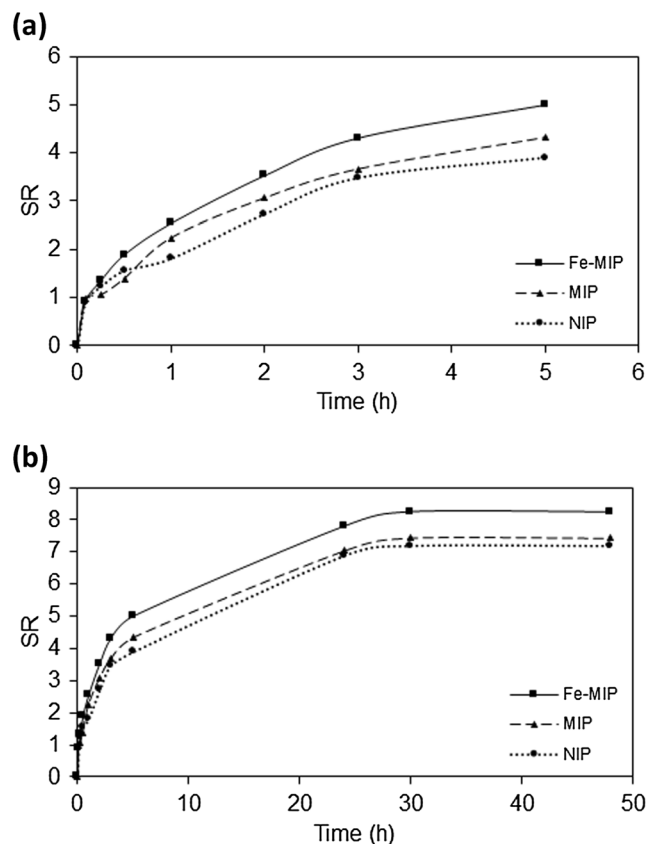

Fig. 6 Swelling diagrams of the samples **a** during 5 h and **b** during 48 h
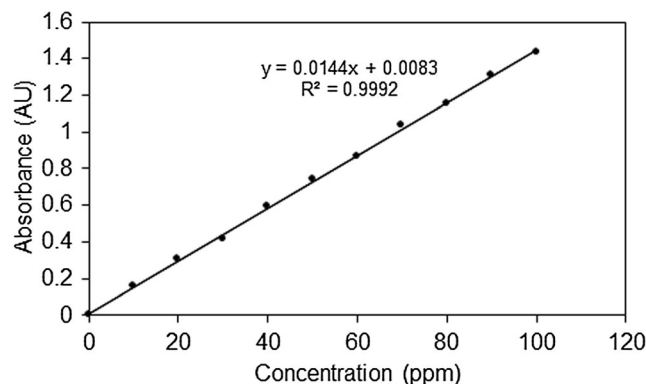
Table 3 ESR and equilibrium binding data of the samples

Sample	ESR	Scatchard analysis		
		Linearity	K_d (µmol l^{-1})	Q_{max} (µmol g^{-1})
Fe-MIP	8.26	$Q/C_s = -0.5783Q + 15.4330^a$	1.73	26.70
		$Q/C_s = -0.0112Q + 4.0723^b$	89.29	363.62
MIP	7.44	$Q/C_s = -0.3381Q + 9.5319^a$	2.96	28.21
		$Q/C_s = -0.0089Q + 3.3568^b$	112.36	377.17
NIP	7.20	$Q/C_s = -0.0135Q + 3.7764$	74.07	279.72

[a] High affinity sites

[b] Low affinity sites

(a)

(b)

(c)
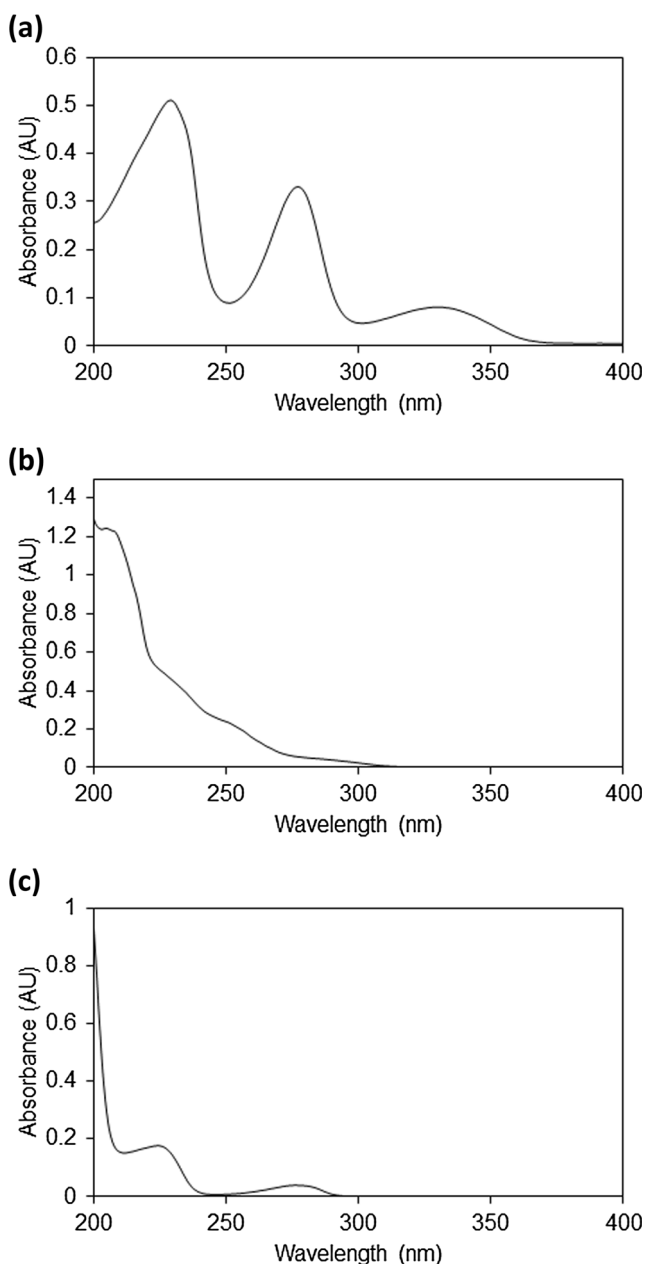
Fig. 7 UV-Vis spectra of **a** FR, **b** MD, and **c** SL

Fig. 8 Calibration curve of FR at 330 nm

The binding isothermal curves of the samples in various concentrations of FR are shown in Fig. 9. It is indicated that the adsorption capacities of the polymers increased with the increasing of the FR initial concentration. As shown in this figure, the Fe-MIP showed higher binding capacity than the MIP and the NIP indicating the higher affinity of this polymer toward the template. Moreover, due to its non-specific binding sites, the NIP showed the lowest binding capacity in various concentrations of the template.

The Scatchard plots of the samples are shown in Fig. 10. The two distinct linear portions with different slopes in the Scatchard plots of the Fe-MIP and the MIP (Fig. 10a, b) indicate that there are two kinds of binding sites present in the polymer structure: specific binding sites and non-specific binding sites. The specific binding sites with a lower K_d value (left part of the Scatchard plot) have higher binding energy and higher affinity toward the template while non-specific binding sites with a higher K_d value (right part of the Scatchard plot) have lower binding energy and lower affinity toward the template. This is a usual phenomenon in Scatchard analysis and shows that there are two different kinds of interactions between the functional monomer and the template molecule in MIP samples. One interaction occurs in cavities with a particular frame which acts as a memory for the template and other interaction which occurs in holes that were not particularly framed during the polymerization process. As
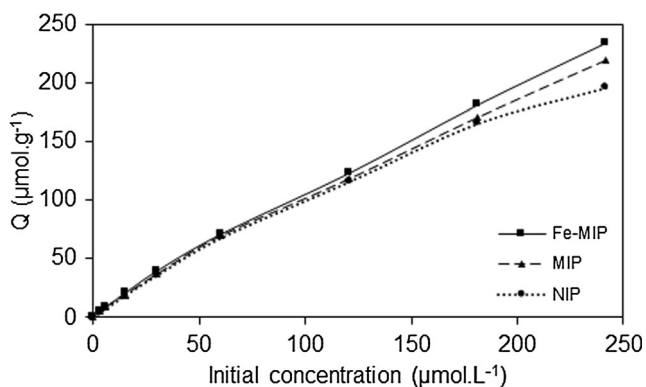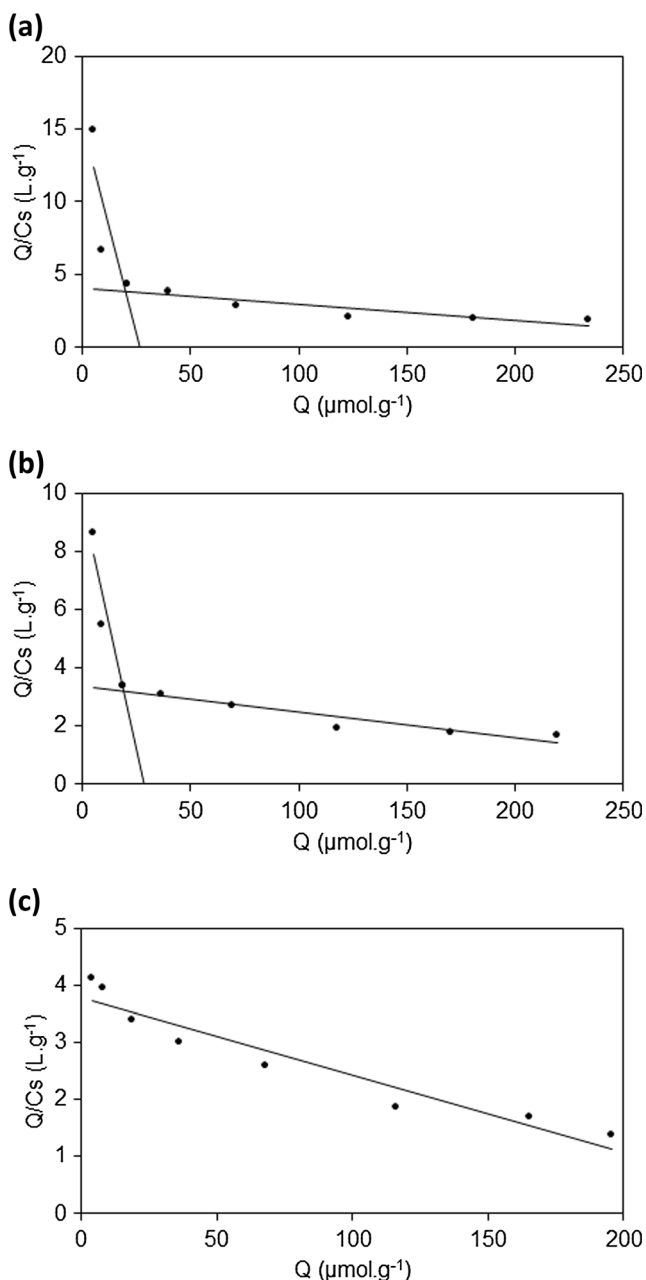
Fig. 9 Binding isotherms of the samples

Fig. 10 Scatchard plots of a Fe-MIP, b MIP, and c NIP

expected, the NIP does not have this character; therefore, the Scatchard plot of this sample showed only one linear regression (Fig. 10c) indicating that there is only one type of binding sites in the polymer structure. The Scatchard analysis data were calculated for all of the samples and are summarized in Table 3. From the K_d and Q_{max} values shown in this table, it is obvious that although the number of high affinity sites in the MIP structure is slightly more than that of the Fe-MIP, their affinity toward the template is lower than Fe-MIP's high affinity sites (higher K_d value). Therefore, the MIP has a weaker ability to adsorb the template than the Fe-MIP.

Selectivity studies

To estimate the equilibrium concentration of each drug in both binary and ternary mixtures, the MCR-LS method was employed. The required data matrix (6×180) was created by placing the spectra of mixtures and standard solutions of the pure drugs beneath each other. Non-negativity constraint was applied on both concentration and spectral profiles while equality constraint was applied only on spectral profiles. Decomposition of data matrix led to determine the concentration of each component in its corresponding solution.

During the Fe-MIP synthesis process, the Fe^{3+} ions were acting as the mediator to keep the main functional monomer (AA) and the template (FR) together by forming a ternary complex. This complex formation enhances the pre-assembly of the AA around the template, compared to the hydrogen bonding between functional monomer and template in conventional methods. Therefore, the cavities formed after the template and the mediator removal from the resulting Fe-MIP structure leads to a more compatible shape structure for the template. Hence, the selectivity of the Fe-MIP for the template toward other components in competitive media increases, compared to the MIP.

Table 4 shows the K_D values of each component in competitive media. According to this table, FR has higher K_D values toward other components in the presence of the Fe-MIP and the MIP, meaning the higher affinity of the template to interact with the sorbent. However, by comparing the FR K_D values for the Fe-MIP and the MIP, it is clearly observable that the values for the Fe-MIP are more than those of the MIP. Therefore, the migration trend of the template to the Fe-MIP is more than the MIP. Unlike the Fe-MIP and the MIP, in the solutions containing the NIP, besides lower K_D values of the template, these values are even less than those of MD in both FR-MD binary and FR-MD-SL ternary mixtures. This is a key factor that shows that the NIP is not particularly framed for any of the components.

The k values of FR toward other components in different solutions are shown in Table 5. For the values which are more than unity, it means that the inclination of the sorbent to adsorb the template is more than the other component and vice versa.

Table 4 Distribution constant values for each component in different solutions in the presence of the samples

Sample	Component	K_D (l g^{-1})		
		FR-MD Binary mixture	FR-SL Binary mixture	FR-MD-SL Ternary mixture
Fe-MIP	FR	3.64	2.90	3.70
	MD	0.38	–	0.09
	SL	–	0.04	0.02
MIP	FR	1.60	2.81	1.89
	MD	0.65	–	0.91
	SL	–	0.47	0.28
NIP	FR	1.40	1.23	1.59
	MD	1.47	–	1.71
	SL	–	0.61	0.76

Table 6 Relative selectivity coefficient values of FR for the imprinted samples against the NIP in different solutions

Sample	k'			
	Binary mixtures		Ternary mixture	
	FR/MD	FR/SL	FR/MD	FR/SL
Fe-MIP	10.08	35.89	44.20	88.52
MIP	2.59	2.96	2.24	3.23

Moreover, the higher the k value is, the more selective is the polymer for the template toward the other components. For the solutions containing the Fe-MIP, the values are remarkably more than that of those of the MIP, demonstrating the higher selectivity of the Fe-MIP toward the template. For the NIP, the k values are less than those for the two MIPs, and for the case for MD, the k values are less than unity meaning that the polymer has tend to adsorb the other component, not the template molecule. Therefore, the NIP does not have a selective behavior for the template in the presence of the other components.

In order to compare the efficiency of the two MIPs for selective separation of the template in competitive media against the NIP, the k' values were also calculated and are shown in Table 6. Similar to that of the k values, the higher the k' value is, the more selective is the imprinted polymer against its corresponding non-imprinted polymer for the template toward the other component. According to Table 6, in all of the cases, the Fe-MIP has a remarkable difference in the k' values toward the MIP, demonstrating that the prepared Fe-MIP is more efficient than the conventionally prepared MIP.

Figure 11 shows the adsorption histograms of each component in different solutions in the presence of the polymers. As

Table 5 Selectivity coefficient values of FR toward other components for each of the samples in different solutions

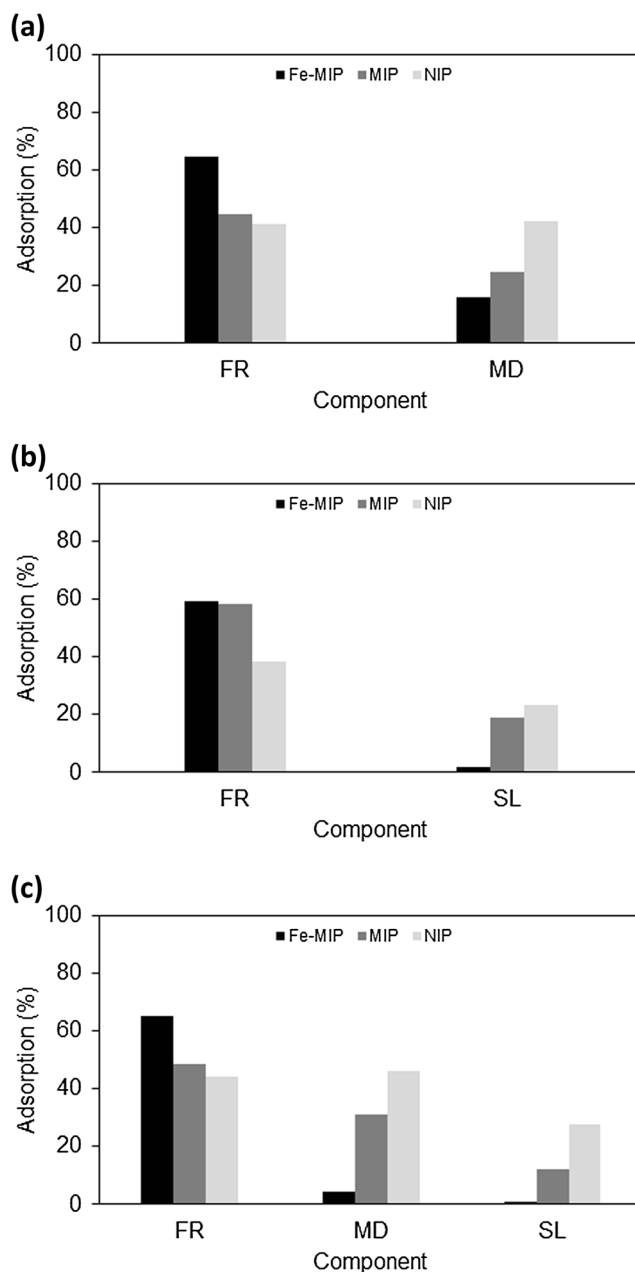| Sample	k			
	Binary mixtures		Ternary mixture	
	FR/MD	FR/SL	FR/MD	FR/SL
Fe-MIP	9.58	72.50	41.11	185.00
MIP	2.46	5.98	2.08	6.75
NIP	0.95	2.02	0.93	2.09

Fig. 11 Adsorption percentage of components in **a** FR-MD binary mixture, **b** FR-SL binary mixture, and **c** FR-MD-SL ternary mixture

Table 7 LC% and imprinting data of the samples

Sample	LC%	P (l g^{-1})	IF
Fe-MIP	22	0.49 × 10^{-1}	1.81
MIP	17	0.30 × 10^{-1}	1.11
NIP	16	0.27 × 10^{-1}	–

Table 8 Drug release data of the samples at the equilibrium state

Sample	Maximum FR release		
	%	ppm	mg
Fe-MIP	92.50	81.44	4.07
MIP	82.06	55.81	2.79
NIP	90.94	58.10	2.91

this figure shows, the adsorption of FR as the template molecule to the Fe-MIP is tangibly more than that of the MIP and the NIP, indicating the successful preparation of the metal ion-mediated MIP.

### Drug loading and in vitro release studies

The LC% values and imprinting data of the polymers are shown in Table 7. As the LC% values show, the Fe-MIP has larger LC% than the other two samples. This can be attributed firstly to its higher SR and ESR than those of the MIP and the NIP which was discussed in the "Swelling studies" section. Also, the presence of specific binding sites in the polymer structure ("Equilibrium binding studies" section) is the other factor of having larger LC% which means that the polymer has higher tendency to adsorb FR. Likewise, the LC% values

Fig. 12 Drug release profiles of the samples **a** during 8 h and **b** during 48 h

of the other two samples can be explained according to "Swelling studies" and "Equilibrium binding studies" sections. Moreover, the partition coefficient (P) values for each of the polymers were calculated according to their LC%, and the IFs of the imprinted samples were further calculated (Table 7). According to the IF values, the Fe-MIP with a higher IF value than the MIP has superior binding properties for FR.

Figure 12 shows the in vitro release profiles of FR during 8 h and 2 days, respectively. Also the maximum drug release data of the samples are summarized in Table 8. As shown in Fig. 12b, the samples reached to their equilibrium state after 2 days (no more drug release over time), but the maximum drug release percentages were different for each of the polymers. According to LC% values, as expected, the Fe-MIP with the largest LC% released the highest amount of drug at its equilibrium state. Surprisingly, the NIP released a higher amount of drug than the MIP, although it had lower LC% than that of the MIP. This phenomenon is attributed to the lower inclination of the NIP to hold the drug, since its cavities are not particularly framed for the template, compared to the MIP (the presence of specific binding sites with lower K_d values in the MIP structure, see the "Equilibrium binding studies" section). Another key point which should be mentioned here is to control the drug release rate especially at its early stages. To reach a suitable slow-release drug delivery system, it is important to restrain the drug release rate and prevent rapid diffusion of the drug (so-called burst release). As shown in Fig. 12a, the Fe-MIP and the MIP have more controlled drug release rate than the NIP which has a sudden drug release at the early stages. This can also be attributed to the higher inclination of imprinted samples to hold the drug due to their specific binding sites; thus, they release the drug rather gently. By comparing the Fe-MIP and the MIP, the Fe-MIP with larger LC% and higher amount of released drug at the equilibrium state is a much more appropriate drug carrier for FR.
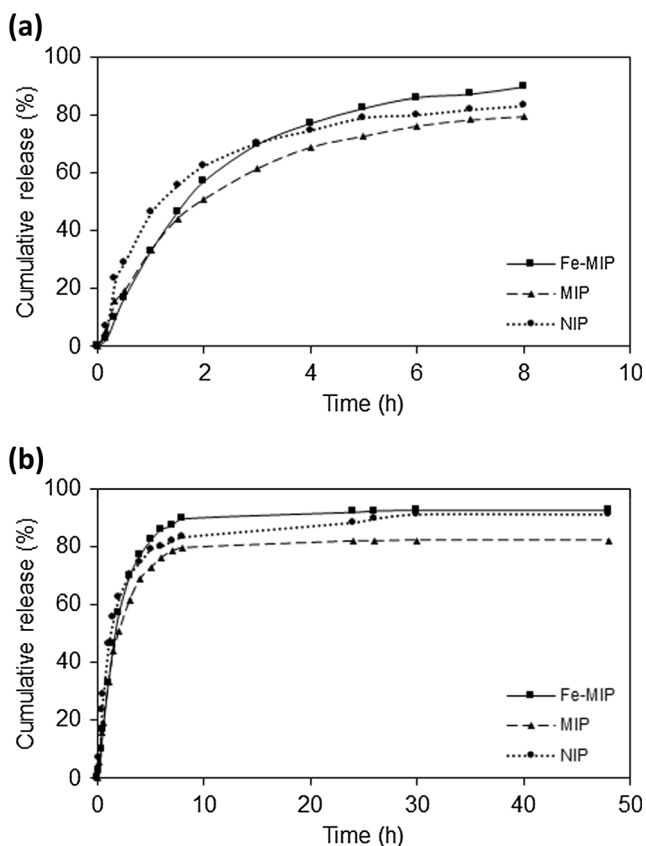
Conclusion

In this study, a Furosemide-imprinted drug delivery system was synthesized and characterized using metal ion mediator in H$_2$O/THF medium. Acrylic acid (AA), acrylamide (AAm),

and N,N'-methylenebis(acrylamide) (MBAAm) were used as functional monomer, comonomer, and cross-linking agent, and also, Fe^{3+} was used as mediator, respectively. Different binding and selectivity parameters of the prepared carrier were calculated and compared with the corresponding metal ion-free MIP and non-imprinted polymer. Results showed higher efficiency in binding and selectivity for the Fe^{3+}-mediated MIP (Fe-MIP). Moreover, the loading and in vitro release capacity of the prepared system were studied and compared with the two other corresponding samples. According to the drug release results, the Fe-MIP showed a larger drug loading capacity and a higher amount of drug release at its equilibrium state. Moreover, the drug release rate of the Fe-MIP was more controlled than that of the MIP and the NIP, especially at the early stages of release.

Compliance with ethical standards

Conflict of interest The authors declare that they have no conflict of interest.

References

1. Manesiotis P, Osmani Q, McLoughlin P (2012) An enantio-selective chromatographic stationary phase for S-ibuprofen prepared by stoichiometric molecular imprinting. J Mater Chem 22:11201–11207

2. Mergola L, Scorrano S, Del Sole R, Lazzoi MR, Vasapollo G (2013) Developments in the synthesis of a water compatible molecularly imprinted polymer as artificial receptor for detection of 3-nitro-L-tyrosine in neurological diseases. Biosens Bioelectron 40:336–341

3. Cheong WJ, Yang SH, Ali F (2013) Molecular imprinted polymers for separation science: a review of reviews. J Sep Sci 36:609–628

4. Caro E, Marcé RM, Cormack PAG, Sherrington DC, Borrull F (2006) Novel enrofloxacin imprinted polymer applied to the solid-phase extraction of fluorinated quinolones from urine and tissue samples. Anal Chim Acta 562:145–151

5. Benito-Peña E, Martins S, Orellana G, Moreno-Bondi MC (2009) Water-compatible molecularly imprinted polymer for the selective recognition of fluoroquinolone antibiotics in biological samples. Anal Bioanal Chem 393:235–245

6. Haupt K (2003) Imprinted polymers—tailor-made mimics of antibodies and receptors. Chem Commun 2:171–177

7. Puoci F, Iemma F, Picci N (2008) Stimuli-responsive molecularly imprinted polymers for drug delivery: a review. Curr Drug Del 5:85–96

8. Gómez-Pineda LE, Pina-Luis GE, Cuán Á, García-Calzón JA, Díaz-García ME (2011) Physico-chemical characterization of flavonol molecularly imprinted polymers. React Funct Polym 71:402–408

9. Li J, Zhang X, Liu Y, Tong H, Xu Y, Liu S (2013) Preparation of a hollow porous molecularly imprinted polymer using tetrabromobisphenol A as a dummy template and its application as SPE sorbent for determination of bisphenol A in tap water. Talanta 117:281–287

10. Luo W, Zhu L, Yu C, Tang H, Yu H, Li X, Zhang X (2008) Synthesis of surface molecularly imprinted silica micro-particles in aqueous solution and the usage for selective off-line solid-phase extraction of 2,4-dinitrophenol from water matrixes. Anal Chim Acta 618:147–156

11. Inoue N, Ooya T, Toshifumi T (2013) Hydrophilic molecularly imprinted polymers for bisphenol A prepared in aqueous solution. Microchim Acta 180:1387–1392

12. He D, Zhang X, Gao B, Wang L, Zhao Q, Chen H, Wang H, Zhao C (2014) Preparation of magnetic molecularly imprinted polymer for the extraction of melamine from milk followed by liquid chromatography-tandem mass spectrometry. Food Control 36:36–41

13. Qu S, Wang X, Tong C, Wu J (2010) Metal ion mediated molecularly imprinted polymer for selective capturing antibiotics containing beta-diketone structure. J Chromatogr A 1217:8205–8211

14. Qu G, Zheng S, Liu Y, Xie W, Wu A, Zhang D (2009) Metal ion mediated synthesis of molecularly imprinted polymers targeting tetracyclines in aqueous samples. J Chromatogr B 877:3187–3193

15. Limmer F, Schinner E, Castrop H, Vitzthum H, Hofmann F, Schlossmann J (2015) Regulation of the Na^+-K^+-$2Cl^-$ cotransporter by cGMP/cGMP-dependent protein kinase I after furosemide administration. FEBS J 282:3786–3798

16. Owen DRJ, MacAllister R, Sofat R (2015) Intravenous furosemide for acute decompensated congestive heart failure: what is the evidence? Clin Pharmacol Ther 98:119–121

17. Cheng HWB, Sham MK, Chan KY, Li CW, Au HY, Yip T (2014) Combination therapy with low-dose metolazone and furosemide: a "needleless" approach in managing refractory fluid overload in elderly renal failure patients under palliative care. Int Urol Nephrol 46:1809–1813

18. Franz CC, Hildbrand C, Born C, Egger S, Bravo AER, Krähenbühl S (2013) Dose adjustment in patients with liver cirrhosis: impact on adverse drug reactions and hospitalizations. Eur J Clin Pharmacol 69:1565–1573

19. Vigil-De Gracia P, Dominguez L, Solis A (2014) Management of chronic hypertension during pregnancy with furosemide, amlodipine or aspirin: a pilot clinical trial. J Maternal Fetal Neonatal Med 27:1291–1294

20. Pourzitaki C, Tsaousi G, Manthou ME, Karakiulakis G, Kouvelas D, Papakonstantinou E (2016) Furosemide modifies heart hypertrophy and glycosaminoglycan myocardium content in a rat model of neurogenic hypertension. Eur J Pharmacol 784:155–163

21. Lin BM, Curhan SG, Wang M, Eavey R, Stankovic KM, Curhan GC (2016) Hypertension, diuretic use, and risk of hearing loss. Am J Med 129:416–422

22. Meka L, Kesavan B, Kalamata VN, Eaga CM, Bandari S, Vobalaboina V, Yamsani MR (2009) Design and evaluation of polymeric coated minitablets as multiple unit gastroretentive floating drug delivery systems for furosemide. J Pharm Sci 98:2122–2132

23. Darandale SS, Vavia PR (2012) Design of a gastroretentive mucoadhesive dosage form of furosemide for controlled release. Acta Pharm Sin B 2:509–517

24. Gholivand MB, Khodadadian M, Ahmadi F (2010) Computer aided-molecular design and synthesis of a high selective molecularly imprinted polymer for solid-phase extraction of furosemide from human plasma. Anal Chim Acta 658:225–232

25. Mohammadi-khoo S, Najafi Moghadam P, Fareghi AR, Movagharnezhad N (2016) Synthesis of a cellulose-based hydrogel network: characterization and study of urea fertilizer slow release. J Appl Polym Sci 133:42935

26. Suo A, Qian J, Yao Y, Zhang W (2007) Synthesis and properties of carboxymethyl cellulose-graft-poly(acrylic acid-co-acrylamide) as a novel cellulose-based superabsorbent. J Appl Polym Sci 103:1382–1388

27. Wu F, Zhang Y, Liu L, Yao J (2012) Synthesis and characterization of a novel cellulose-g-poly(acrylic acid-co-acrylamide) superabsorbent composite based on flax yarn waste. Carbohydr Polym 87: 2519–2525

28. Haseeb MT, Hussain MA, Yuk SH, Bashir S, Nauman M (2016) Polysaccharides based superabsorbent hydrogel from linseed: dynamic swelling, stimuli responsive on–off switching and drug release. Carbohydr Polym 136:750–756